Bulletin of Earthquake Engineering (2024) 22:3243–3260
https://doi.org/10.1007/s10518-024-01882-4

ORIGINAL ARTICLE

Ductility demands for stiffness-degrading SDOF systems under pulse-like ground motions of the 2023 Pazarcık (Kahramanmaraş) earthquake

Taner Ucar[1] · **Onur Merter**[2]

Received: 17 October 2023 / Accepted: 22 February 2024 / Published online: 13 March 2024

Abstract
This paper investigates the inelastic displacement ratios (IDRs) and displacement ductility demands of a wide range of single-degree-of-freedom (SDOF) systems subjected to pulse-like ground motions (GMs) of the 2023 Pazarcık (Kahramanmaraş) earthquake. A set of twenty-seven GMs characterized as pulse-like are utilized in the study. As-recorded velocity time histories of horizontal components are rotated over 90° at a step of 1° to attain the waveform with the largest peak ground velocity (PGV) over all horizontal orientations. Inelastic displacement ratio and displacement ductility spectra are computed through nonlinear response history analysis (RHA). Local amplifications of both spectra are observed at some periods. The results of this study show that large inelastic displacement and ductility demands are imposed on certain reinforced concrete (RC) structures. Finally, predictive models of the mean inelastic displacement ratio and mean ductility demand spectra (DDS) are developed based on the Gauss–Newton algorithm (GNA). The model provides a strong correlation between the computed and the estimated data, and sufficient convergence criteria. The results of this study collectively emphasize the necessity of integrating pulse-like GMs into future revisions of earthquake codes.

Keywords Pulse-like ground motions · Stiffness-degrading systems · Inelastic displacement ratios · Ductility demand spectra (DDS) · Predictive model

1 Introduction

Several existing RC buildings exhibited inadequate performance during the seismic events in the Kahramanmaraş earthquake sequence. The two most significant seismic events in the sequence were the M_w 7.7 Pazarcık and the M_w 7.6 Elbistan earthquakes, which were

✉ Taner Ucar
taner.ucar@deu.edu.tr

Onur Merter
onur.merter@ieu.edu.tr

[1] Department of Architecture, Dokuz Eylül University, Izmir, Turkey

[2] Department of Civil Engineering, Izmir University of Economics, Izmir, Turkey

highly destructive. The predominant building inventory within the region affected by these seismic events primarily consists of RC residential structures. The post-yield behavior of RC structural members is considerably different from that of steel structural members. Despite the absence of apparent strength loss, RC structural members are anticipated to demonstrate a certain degree of stiffness degradation during cyclic load reversals, attributed to factors such as cracking and loss of steel–concrete bond (FEMA P440A 2009).

Within the causative fault, 379 strong-motion stations of the National Strong Motion Network operated by the Disaster and Emergency Management Presidency have successfully recorded a large number of both far-field and near-source strong-motion waveforms during the 2023 Pazarcık (Kahramanmaraş) earthquake (AFAD 2023). Among the near-source records, several GMs have been characterized as pulse-like as a result of the investigations for potential pulse-like features (Baltzopoulos et al. 2023; Wu et al. 2023). At present, there is a wide consensus that pulse-like GMs impose larger inelastic displacement demands on structures inducing more severe damage (i.e. resulting in significant permanent deformations) than non-impulsive GMs. The problem is that the imposed large inelastic deformations may cause loss of stiffness in RC structural members influencing the response of the building to GMs.

Many studies have been conducted on the seismic response of stiffness-degrading systems to ordinary GMs. Chopra and Kan (1973) investigated the inelastic earthquake response of multi-story RC buildings by considering the effects of stiffness degradation. The influence of prior earthquake damage on the peak displacement response of stiffness-degrading systems was studied by Aschheim and Black (1999). Song and Pincheira (2000) computed inelastic displacement demands of stiffness- and strength-degrading systems. They also studied displacement demands of SDOF systems subjected to near-fault ground motions (NFGMs) (Pincheira and Song 2000). Pekoz and Pincheira (2004) conducted a parametric study to investigate the effect of strength and stiffness degradation on the earthquake response of SDOF systems and a predictive equation for the displacement amplification factor of degrading systems is proposed. Peak displacement demands of SDOF degrading and non-degrading systems subjected to forward-directivity NFGMs were evaluated and a predictive equation was proposed by Ruiz-García (2011). Soil-structure interaction effects on several structural parameters such as strength reduction factor and inelastic displacement ratio (IDR) for stiffness-degrading systems built on soft soils were studied by Aydemir (2013a, b). Ganjavi et al. (2018) developed response modification factors for stiffness-degrading soil-structure systems. Hassani et al. (2018) investigated the influence of soil-structure interaction on IDRs of degrading systems by considering four different hysteretic models.

The studies related to inelastic displacement demands of stiffness-degrading systems under pulse-like GMs are very limited (Wen et al. 2014; Li et al. 2020c), whereas the effects of pulse-like GMs on seismic demands imposed on non-degrading systems are studied thoroughly. Sehhati et al. (2011) employed Incremental Dynamic Analysis (IDA) to assess the effects of pulse-like forward-directivity GMs on multi-story structures. Wen et al. (2014) computed IDRs for the NF pulse-like GMs and statistically evaluated the effect of several parameters, where the structural degrading behavior is also evaluated. An analytical model for near-source pulse-like seismic demands was developed by Baltzopoulos et al. (2016). Lu et al. (2018) developed a displacement-based framework for the seismic design of flexible-base structures under pulse-like GMs. Ji et al. (2019) concluded that large ductility demand and the bottom soft-story mechanism were the main reasons for the structural damage under pulse-like GMs of the Hualien earthquake. The effects of forward directivity on seismic demands in RC frames were investigated based

on the results obtained from nonlinear time-history analyses by Li et al. (2020a). Reyes and Kalkan (2012) used in their study Baker's (2007) numerical procedure to identify and characterize velocity pulses in rotated motions. Kalkan and Reyes (2015) suggested that individual ground motions rotated to have maximum directions for the maximum response values do not always provide conservative engineering demand parameters. However, Li et al. (2020b) presented a simple yet efficient method to identify the orientation of the strongest velocity pulses. They demonstrated that pulse-like GMs in the orientation with the maximum PGV produce the largest mean ductility demand. Dong et al. (2022) constructed ductility demand spectra (DDS) for self-centering structures under NF pulse-like GMs and investigated the effects of GM and structural characteristics on the spectra. NF pulse seismic ductility spectra based on machine learning were developed and applied to obtain the optimal longitudinal reinforcement ratio of bridge columns (Yang et al. 2023).

The two notable earthquake sequences with M_w 7.7 and 7.6 occurred in Pazarcık and Elbistan (Kahramanmaraş) Türkiye on February 6, 2023, at 04:17 (01:17 GMT) and 10:24 (07:24 GMT). The depth of the first event is 8.6 km and the epicentre is located at 37.288° N, 37.043° E. The second earthquake with the epicentre at 38.089° N, 37.239° E occurred 9 h after the first one and its depth is reported as 7 km (AFAD 2023). There are several studies in the literature that investigate this 2023 earthquake doublet in south-eastern Türkiye. However, these studies generally concentrate on strong ground motion characteristics and the preliminary investigation of building damage (Işık et al. 2023; Ozkula et al. 2023; Ozturk et al. 2023; Sagbas et al. 2023; Tao et al. 2023; Wu et al. 2023). Actually, they do not investigate the structural response parameters inducing the damage. On the other hand, there exists a close relation between structural damage and ductility factor (Farrow and Kurama 2004; Akkar and Miranda 2005; Yi et al. 2007). In addition, a considerable number of pulse-like GMs, which are of earthquake engineering interest since they impose more severe inelastic demands on certain structures than non-impulsive GMs, was recorded during the 6 February 2023 M_w 7.7 Pazarcık (Kahramanmaraş) earthquake.

The present study contributes to the literature by computing displacement ductility demands for stiffness-degrading SDOF systems under pulse-like GMs of the 2023 Pazarcık (Kahramanmaraş) earthquake and investigating the ductility factors that induce substantial structural damage and collapse in the regions affected by this devastating event. Predictive models for the mean inelastic displacement ratio and mean ductility demand spectra (DDS) have been formulated utilizing the Gauss–Newton algorithm. The results are presented as a family of inelastic displacement ratio and ductility demand curves (i.e., spectra) derived for six levels of lateral strength ratios. Finally, simple but efficient predictive models for both spectra, where GNA is employed to solve the nonlinear regression problem, are established.

2 Pulse-like ground motions used in the study

2.1 Ground motions

The present study utilizes a set of twenty-seven pulse-like GMs developed by Baltzopoulos et al. (2023) and Wu et al. (2023). These twenty-seven pulse-like GMs were downloaded once again from AFAD's (2023) database by the authors and used in the study. A total of 379 three-component acceleration records were provided by AFAD during the 2023 Pazarcık (Kahramanmaraş) earthquake. Baltzopoulos et al. (2023) and Wu et al. (2023)

examined these ground motion waveforms for potential pulse-like features. Wu et al. (2023) selected records from stations with epicentral distances (R_{epi}) less than 200 km, whereas Baltzopoulos et al. (2023) used records with Joyner-Boore distances (R_{JB}) less than 20 km. In both studies, candidate pulse waveforms were extracted from the velocity time histories by using the wavelet transform. A pulse indicator (PI) taking values between 0 and 1 was assigned to each candidate pulse waveform. Records with PI > 0.85 were classified as pulses by Wu et al. (2023), whereas records with PI > 0.90 were characterized as pulse-like by Baltzopoulos et al. (2023). The additional parameters for the quantitative classification of GMs used in this study as pulse-like are given in Baltzopoulos et al. (2023) and Wu et al. (2023). The map of the stations for the pulse-like GMs is given in Fig. 1 (AFAD 2023).

2.2 Orientation of the strongest velocity pulses

Ground motion time histories are inherently nonstationary signals. Accordingly, the strongest pulse-like features might be observed in any orientation (Ji et al. 2019). Li et al. (2020b) assumed that pulse-like GMs contain the strongest pulse in the orientation associated with the maximum PGV. This approach is also postulated in this paper.

Time series of the selected pulse-like GMs have been downloaded from the strong GM database of AFAD. Subsequently, as-recorded velocity time histories for both horizontal components of motion are rotated over 90° at a step of 1° to attain the waveform with the largest PGV over all horizontal orientations.

Two orthogonal GM components can be rotated by an angle θ to obtain the GM in any arbitrary orientation (Boore et al. 2006). Using a rotation matrix this is constructed as

$$\left\{ \begin{array}{c} v_1'(t) \\ v_2'(t) \end{array} \right\} = R(\theta) \left\{ \begin{array}{c} v_1(t) \\ v_2(t) \end{array} \right\} = \left[\begin{array}{cc} \cos\theta & -\sin\theta \\ \sin\theta & \cos\theta \end{array} \right] \left\{ \begin{array}{c} v_1(t) \\ v_2(t) \end{array} \right\} \quad (1)$$

where $v_1(t)$ and $v_2(t)$ represent orthogonal as-recorded velocity time histories, $v_1'(t)$ and $v_2'(t)$ are velocity time histories in any arbitrary orientation θ, and $R(\theta)$ is a counter-clockwise rotation matrix.

Fig. 1 The map of the stations for selected GMs in Table 1 (AFAD 2023)

The details of the pulse-like GMs are listed in Table 1 with the station codes, where V_{S30} is the average shear wave velocity to 30 m depth of subsoil, PGA is the peak ground acceleration and PGV is the peak ground velocity of rotated time series by the angle θ. These accelerograms present PGV ranges between 27.59 and 161.73 cm/s. The ratio of PGV to PGA of the utilized pulse-like GMs varies from 0.11 to 0.586 s, which means that they exhibit remarkably larger PGV/PGA ratios. The pulse-like record of Station 3143 has the highest PGV of 161.73 m/s. It can be seen from the data in Table 1 that Station 3147 gives the highest PGV/PGA ratio although it has the smallest PGA and PGV values.

The waveforms of the records with PGV values exceeding 150 cm/s are shown in Fig. 2 together with the extracted pulses and pulse periods (T_p). The latitude and longitude positions of the recording stations are also provided in the same figure. All these waveforms have been gathered from accelerographic stations placed in Hatay, the southernmost province of Türkiye with an area of 5524 km^2 and a population of 1,686,043 according to the 2022 census data. It is apparent from this figure that the buildings located in the city of Hatay have been enormously subjected to pulse-like GMs. This finding reasonably explains

Table 1 Pulse-like GMs used in this study (AFAD 2023)

No	Station Code	R_{epi} (km)	V_{S30} (m/s)	θ (°)	PGA (g) (rotated)	PGV (cm/s) (rotated)	PGV (cm/s) (non-rotated)	PGV/PGA (s) (rotated)
1	0120	125.25	439	9	0.108	32.32	23.41	0.305
2	2712	29.79	–	52	0.721	138.29	110.06	0.196
3	2715	57.62	–	55	0.364	62.47	55.42	0.175
4	2716	57.38	–	49	0.254	70.45	52.43	0.283
5	2717	57.34	–	58	0.181	60.02	50.77	0.338
6	2718	48.3	–	60	0.659	123.37	116.80	0.191
7	3115	113.57	424	51	0.245	56.49	48.30	0.235
8	3116	105.38	870	44	0.184	49.00	39.74	0.272
9	3123	143	470	90	0.665	186.78	186.78	0.286
10	3124	140.11	283	74	0.597	115.57	112.32	0.197
11	3125	142.15	448	58	0.859	122.39	102.64	0.145
12	3126	143.54	350	25	1.107	119.28	92.71	0.110
13	3129	146.39	447	90	1.378	171.6	171.60	0.127
14	3134	90.29	374	56	0.272	47.55	39.54	0.178
15	3137	82.48	688	43	0.511	105.57	76.85	0.211
16	3139	96.19	272	68	0.627	156.44	145.26	0.254
17	3143	65.13	444	40	0.404	161.73	104.36	0.408
18	3144	77.04	485	23	0.941	144.37	131.44	0.156
19	3145	91.13	533	84	0.692	158.56	157.77	0.234
20	3147	177.12	–	65	0.048	27.59	24.93	0.586
21	4611	55.32	731	68	0.337	44.27	40.85	0.134
22	4615	13.83	484	16	0.618	146.79	131.16	0.242
23	4616	20.54	390	28	0.693	106.19	86.51	0.156
24	4625	28.4	346	67	0.455	82.14	75.63	0.184
25	8002	43.91	430	20	0.248	46.47	38.27	0.191
26	8003	72.18	350	43	0.181	39.75	26.94	0.224
27	NAR	15.35	–	36	0.501	120.14	90.79	0.245

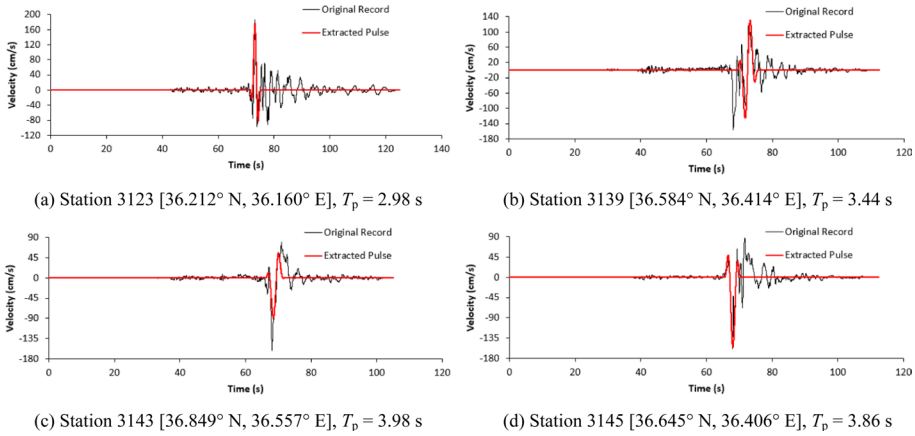

(a) Station 3123 [36.212° N, 36.160° E], T_p = 2.98 s

(b) Station 3139 [36.584° N, 36.414° E], T_p = 3.44 s

(c) Station 3143 [36.849° N, 36.557° E], T_p = 3.98 s

(d) Station 3145 [36.645° N, 36.406° E], T_p = 3.86 s

Fig. 2 Velocity time histories of the rotated records

the significant damage in Hatay caused by the pulse-like GMs of the 2023 Pazarcık (Kahramanmaraş) earthquake. As of 8 April 2023, the province had recorded over 22,000 deaths from the 2023 earthquakes, the highest reported across the 11 earthquake-affected provinces in Türkiye.

3 Response of SDOF systems to pulse-like GMs

3.1 Inelastic displacement ratios (IDRs)

Inelastic displacement ratio (IDR) is defined as the ratio of maximum inelastic displacement demand (u_m) to elastic displacement demand (u_0) of SDOF systems having the same structural and dynamic characteristics when subjected to the same earthquake GM excitation (Baéz and Miranda 2000; Ruiz-Garcia and Miranda 2003; Iervolino et al. 2012). Mathematically this can be expressed as in Eq. (2):

$$C_R = \frac{u_m}{u_0} \tag{2}$$

The maximum inelastic displacement demand in Eq. (2) is computed from the nonlinear RHA of SDOF systems with constant relative lateral strength, which is measured through a yield strength reduction factor (R_y). It is widely accepted that nonlinear RHA is quite time-consuming. Therefore, the inelastic displacement ratio (IDR) is a very useful response parameter since it permits estimating maximum inelastic displacement demands from elastic displacement demands. Briefly, when the inelastic displacement ratio (IDR) is used instead of RHA, maximum inelastic displacement demands can be estimated more practically.

In order to compute inelastic displacement ratios for pulse-like GMs recorded during the 2023 Pazarcık (Kahramanmaraş) earthquake, nonlinear RHA of 5% damped SDOF systems subjected to an ensemble of 27 pulse-like accelerograms are performed using PRISM software (2010). SDOF systems are characterized by their natural period of vibration (T_n) and normalized lateral strength index (i.e., F_y/mg). Six levels of lateral strength ratios (i.e.,

$R_y = 1.5$, 2, 2.5, 3, 3.5, and 4) are implemented. As a result, a wide range of SDOF systems are taken into consideration. It is quite clear that as R_y increases the level of inelasticity increases. Low levels of R_y (e.g., $R_y < 3$) may be referred to as strong systems relative to the GM intensity. On the other hand, large levels of R_y may be referred to as weak systems (i.e., highly inelastic structures). Accordingly, the range of R_y of the study considers several levels of inelasticity and they are reasonably consistent values according to Turkey Building Earthquake Code (TBEC 2018). Similar values of R_y are also used by Ruiz-Garcia (2011) and Ruiz-Garcia and Miranda (2003).

The building stock in areas affected by the 2023 Pazarcık (Kahramanmaraş) earthquake is substantially composed of RC structures. RC structures exhibit stiffness degradation when they are subjected to reversed cyclic loading (Hassani et al. 2018). Accordingly, in this study, the Modified Takeda Hysteresis Model is employed to represent stiffness-degrading systems. This model is extensively used to simulate the nonlinear lateral force—lateral displacement behavior of RC systems under earthquake ground motion-induced loading reversals as shown in Fig. 3. In this model, both the loading and unloading stiffnesses degrade as a function of the previous loading history and they are not the same (Takeda et al. 1970). The post-yielding stiffness ratio (r) of 0.05 and the unloading stiffness ratio (α) of 0.3 are assumed to constitute the force–displacement relationships of the Modified Takeda Hysteresis Model (Fig. 3). In Fig. 3, f_y is the yield strength, u_y is the yield displacement, u_m is the maximum inelastic displacement, u_p is the plastic displacement, k_0 is the initial stiffness, k_u is the unloading stiffness, β is the reloading stiffness ratio, α is the unloading stiffness ratio, and the post-yielding stiffness ratio is indicated by r.

IDRs are primarily computed for individual pulse-like GMs and SDOF systems with T_n values ranging from 0.1 to 3 s. As a part of this study, a total of 4860 IDRs corresponding to 27 pulse-like GMs, 30 discrete periods of vibration, and 6 levels of lateral strength ratios are computed. Due to page limitations, only inelastic displacement ratio spectra (IDRS) for pulse-like GMs with PGVs exceeding 150 cm/s are presented in Fig. 4. As can be seen

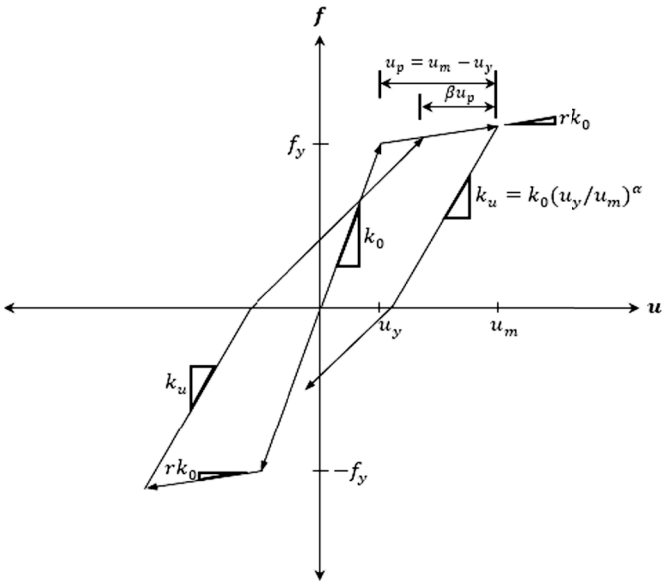

Fig. 3 Modified Takeda degrading stiffness hysteretic model

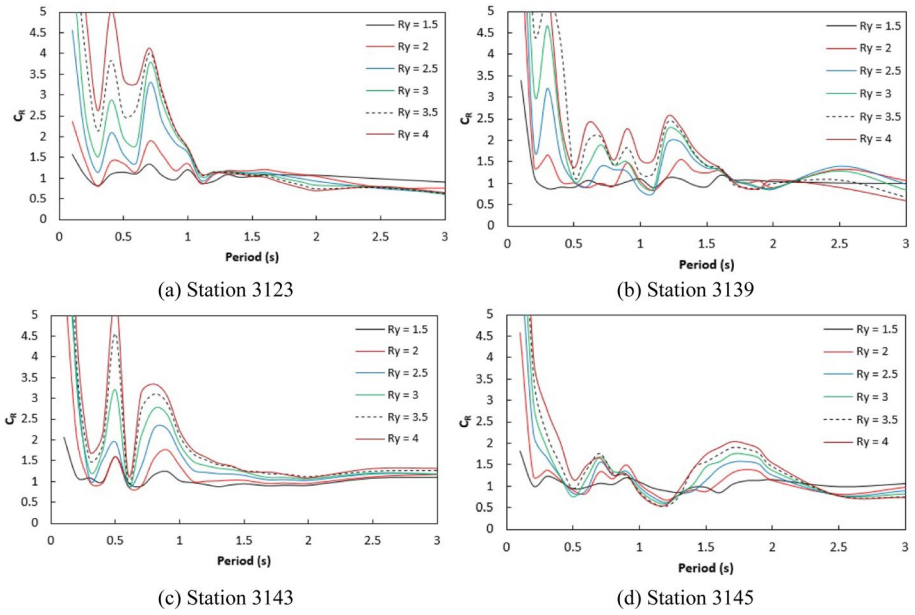

Fig. 4 IDRS for pulse-like GMs with PGVs exceeding 150 cm/s

from the graph, local amplifications of inelastic displacement ratios are observed at some periods shorter than 1.0 s at stations 3123 and 3143. For example, for the SDOF systems with $R_y = 4$, C_R ($T_n = 0.7$ s) = 4.13 and C_R ($T_n = 0.5$ s) = 5.43 are computed, respectively at stations 3123 and 3143. These results indicate that pulse-like GMs recorded at stations 3123 and 3143 impose quite large inelastic displacement demands on short- to medium-period structures. On the other hand, at stations 3139 and 3145, local amplifications are also observed at periods longer than 1.0 s. More clearly, for SDOF systems with $R_y = 4$, C_R ($T_n = 1.2$ s) = 2.55 and C_R ($T_n = 1.7$ s) = 2.04 are computed at stations 3139 and 3145. This finding indicates that large inelastic displacement demands are imposed on long-period structures. The above-explained amplifications are frequently observed at IDRS derived for other pulse-like GMs which are not shown herein.

Mean IDR values are then calculated by averaging the results for each natural period. Figure 5 shows the mean IDRS. The mean IDRs are larger than 1 in the short-period region (for periods smaller than 0.6 s in this study) and increase sharply as the period shortens. It is apparent that the equal displacement rule (EDR) is not acceptable in this period region and inelastic systems have experienced considerably larger lateral displacements than elastic systems. At medium periods, the mean inelastic displacement ratios are moderately dependent on the natural period. In this period region, they are obviously larger than 1 for SDOF systems with $R_y > 1.5$, and approximately equal to 1.0 for SDOF systems with $R_y = 1.5$. In the long-period region, the mean inelastic displacement ratios are larger than 1.0 for highly inelastic systems (e.g., $R_y \geq 3$). It is worth noting that the EDR is not reasonable, particularly for highly inelastic systems. These results are consistent with those of Wen et al. (2014), where IDRs for 81 NFGMs are computed, but the mean IDRs of the present study are greater than those computed by Wen et al. (2014). Wen et al. (2014) have also emphasized that, in the medium period region, the mean IDRs are obviously larger than 1.0 for the weak structures (i.e., highly inelastic structures). Moreover, local amplification of

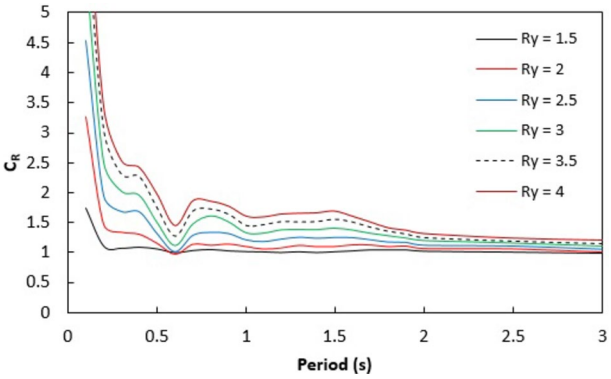

Fig. 5 Mean IDRS

mean IDRs is observed at periods of vibration around 0.7–0.8 s in the present study and it seems to increase as R_y increases.

3.2 Ductility demand spectra (DDS)

Pulse-like GMs usually induce significantly higher displacement and ductility demands on structures than ordinary GMs (Alavi and Krawinkler 2004; Kalkan and Kunnath 2006; Ruiz-García 2011; Sehhati et al. 2011; Iervolino et al. 2012; Wen et al. 2014). Displacement ductility demand can be considered to be one of the representative parameters of structural damage due to large deformations (Li et al. 2020c). This condition prompted our investigation into the displacement ductility spectra of SDOF systems subjected to pulse-like GMs from the 2023 Pazarcık (Kahramanmaraş) earthquake.

The ductility demand spectrum relates peak displacement ductility demands with the natural vibration period or frequency of SDOF systems for constant lateral strength ratios (Hatzigeorgiou 2010; Uçar and Merter 2020; Dong et al. 2022). The ductility demand (μ) is defined as

$$\mu = \frac{u_m}{u_y} \tag{3}$$

where u_y represents the yield displacement of an SDOF system.

Considering the results of the previous section (and considering IDR as in Eq. (2)), yield displacements of SDOF systems subjected to pulse-like GMs of the study are primarily computed as in Eq. (4):

$$u_y = \frac{u_0}{R_y} \tag{4}$$

where R_y is the yield strength reduction factor. In order to define R_y the general strength-displacement relation of an SDOF system according to the equal displacement rule is presented in Fig. 6, where f_e is the elastic strength and f_y is the yield strength. The elastic displacement demand (u_0) is equal to the maximum inelastic displacement demand (u_m) for systems having long natural vibration periods. R_y is the ratio of f_e to f_y, or u_o to u_y.

Afterward, DDS corresponding to specific lateral strength ratios (i.e., $R_y = 1.5$, 2, 2.5, 3, 3.5, and 4) are derived for individual pulse-like GMs. Figure 7 shows DDS for pulse-like

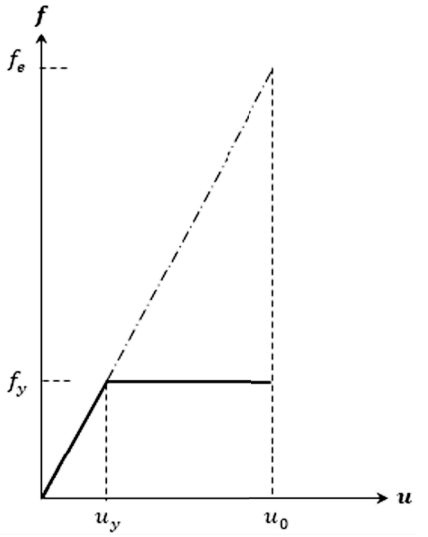

Fig. 6 Strength-displacement (f-u) relation of an SDOF system according to the equal displacement rule

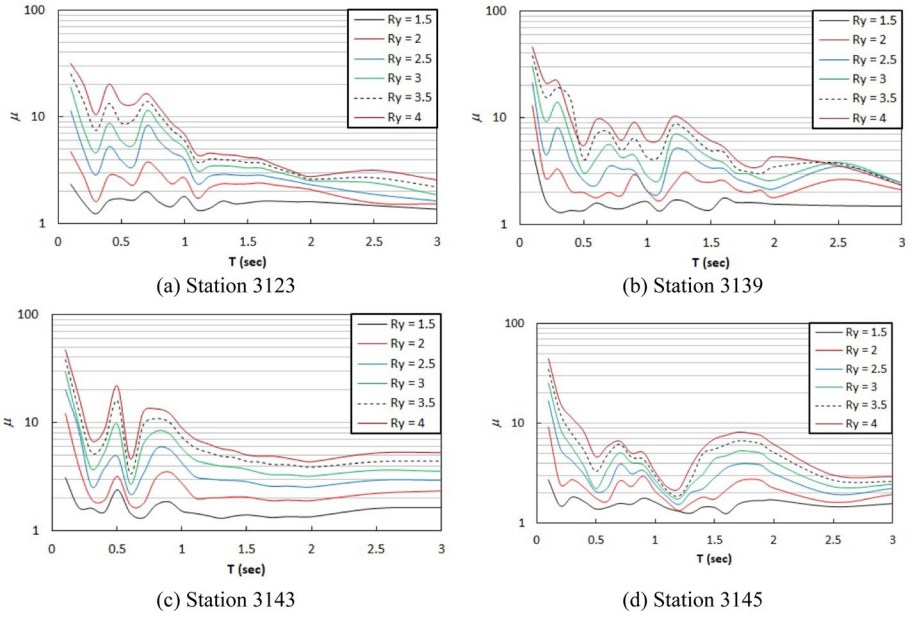

(a) Station 3123 (b) Station 3139

(c) Station 3143 (d) Station 3145

Fig. 7 DDS for pulse-like GMs with PGVs exceeding 150 cm/s

GMs with PGVs exceeding 150 m/s. A logarithmic scale is employed for the vertical axes of DDS since high ductility demands are computed for short periods. No common trend is observed in DDS for individual pulse-like GMs. What stands out in the DDS is the significant local amplifications at medium to long periods. For example, for the SDOF systems with $R_y = 4$, μ ($T_n = 0.4$ s) = 20.18, μ ($T_n = 0.8$ s) = 13.36, and μ ($T_n = 1.7$ s) = 8.13 are computed, at stations 3123, 3143, and 3145, respectively.

Figure 8 presents the mean DDS of inelastic SDOF systems under pulse-like GMs of the 2023 Pazarcık (Kahramanmaraş) earthquake. At short periods, the mean ductility demand spectra (DDS) are strongly dependent on the natural period of the system, regardless of the level of inelasticity. At medium to long periods, a moderate dependence on the natural period is observed, particularly for systems with $R_y > 2$. At long periods, the dependence of the mean DDS on the natural period is no longer observable.

Contrary to expectations, the mean ductility demand spectra (DDS) do not exhibit the common spectral shape, which is very typical for ordinary GMs. Actually, SDOF systems in the acceleration-sensitive region of the spectrum experience high ductility demands, and this variation trend of the spectra is similar to those for ordinary GMs. But at relatively long periods, ductility demands do not exactly approximate lateral strength ratios ($\mu \neq R_y$). This observation is particularly valid for highly inelastic systems (e.g., $R_y \geq 3$). It is clear that the mean DDS are sensitive to lateral strength ratio, and relatively high ductility demands are imposed on highly inelastic systems. Local amplification of mean ductility spectra is observed at periods of vibration around 0.7–0.8 s.

The building stock in areas affected by the 2023 Pazarcık (Kahramanmaraş) earthquake is mainly composed of RC buildings and substantial damage and collapse of many of these buildings were observed in the areas affected by this devastating earthquake. RC buildings seismically designed in accordance with the provisions of TBEC (2018) are expected to exhibit ductility demands of 2.5–3. Earthquake load reduction coefficient relies on the fact that the RC building will behave ductile. However, damage observations of RC buildings from 2023 Kahramanmaraş earthquake sequence revealed that a significant portion of RC buildings were not able to develop the presumed ductility level (Vuran et al. 2024). In addition, as shown in the present study, pulse-like GMs recorded during the 2023 Pazarcık (Kahramanmaraş) earthquake have imposed large IDRs and ductility demands on the buildings. The imposed IDRs and ductility demands were not adequately estimated in the seismic design stage since the EDR may result in significant underestimations of the maximum inelastic displacement demands of pulse-like GMs. Evaluating the IDRs and the ductility demands computed in the present study may lead to understanding the substantial damage and collapse of several RC buildings resulting from the 2023 Pazarcık (Kahramanmaraş) earthquake.

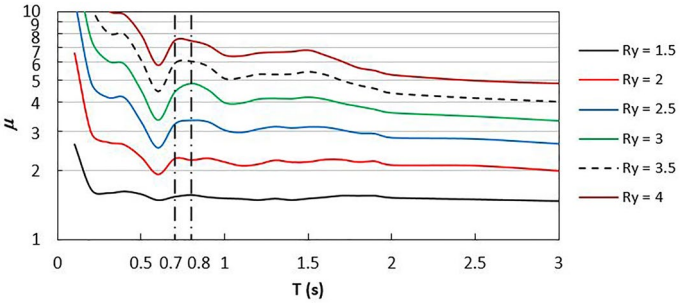

Fig. 8 Mean DDS

4 Predictive models for inelastic displacement ratio and ductility demand spectra

In order to approximate their spectral shapes, predictive models of both mean inelastic displacement ratio and mean ductility demand spectra (DDS) based on the GNA are established. This algorithm was previously applied for estimating constant-ductility energy factor spectra of near- and far-fault GMs by the Authors (Ucar and Merter 2022).

A three-parameter exponential equation for each considered lateral strength ratio is proposed for relating the mean inelastic displacement ratio or the mean ductility demand spectra (DDS) to a structural period:

$$C_R(T) \text{ or } \mu(T) = \left(a_0 e^{-a_1 T} + a_2\right) + \varepsilon \tag{5}$$

where a_0, $a_{1,}$ and a_2 are constant parameters to be determined and ε is the residual between the computed and the estimated values.

GNA is an effective method for minimizing the residuals between the computed and estimated data such the estimated values are in good agreement with the available data. It is a method for finding the minimum of a non-linear function. The compact form of the model is:

$$\left(C_R\right)_i \text{ or } (\mu)_i = f\left(T_i\right) + \varepsilon_i \tag{6}$$

where C_R or μ is the vector function of T, subscript i represents the discrete data, and T is a vector of n-dimension.

Expanding the above equation to Taylor series about a_0, $a_{1,}$ and a_2 (i.e., the constant parameters) and not taking into account the higher derivative terms, Eq. (7) is derived for a three-parameter exponential model:

$$f\left(T_i\right)_{k+1} = f\left(T_i\right)_k + \frac{\partial f\left(T_i\right)_k}{\partial a_0}\Delta a_0 + \frac{\partial f\left(T_i\right)_k}{\partial a_1}\Delta a_1 + \frac{\partial f\left(T_i\right)_k}{\partial a_2}\Delta a_2 \tag{7}$$

where k represents the iteration step, Δa_0, Δa_1 and Δa_2 are the difference between the iteration steps.

Substituting Eqs. (7) into (6) yields

$$\left[\left(C_R\right)_i \text{ or } (\mu)_i\right] - f\left(T_i\right)_k = \frac{\partial f\left(T_i\right)_k}{\partial a_0}\Delta a_0 + \frac{\partial f\left(T_i\right)_k}{\partial a_1}\Delta a_1 + \frac{\partial f\left(T_i\right)_k}{\partial a_2}\Delta a_2 + \varepsilon_i \tag{8}$$

Equation (8) can be represented by a matrix notation as is Eq. (9):

$$\{D\} = \left[J_k\right]\{\Delta A\} + \{\varepsilon\} \tag{9}$$

where $\{D\}$ is n-dimensional vector of differences between the computed and the estimated data, $\left[J_k\right]$ is $n \times 3$ dimensional Jacobian matrix of partial derivatives, $\{\Delta A\}$ is a vector of 3×1, and $\{\varepsilon\}$ is n-dimensional vector of residuals.

The following matrix equation is obtained as a result of implementing the Least-Square Method on Eq. (9):

$$\{\Delta A\} = \left(\left[J_k\right]^{\mathrm{T}}\left[J_k\right]\right)^{-1}\left(\left[J_k\right]^{\mathrm{T}}\{D\}\right) \tag{10}$$

where superscript T denotes the matrix transpose.

Table 2 Results of non-linear regression analysis for IDRS

R_y	a_0	a_1	a_2	$\lvert\varepsilon_0\rvert$	$\lvert\varepsilon_1\rvert$	$\lvert\varepsilon_2\rvert$	R^2
1.5	5.602	20.466	1.022	0.000047	0.000023	0.000000	0.98771
2	10.525	15.818	1.102	0.000024	0.000015	0.000001	0.98916
2.5	11.709	12.707	1.227	0.000044	0.000033	0.000002	0.98335
3	12.886	10.999	1.353	0.000042	0.000035	0.000003	0.98336
3.5	13.312	9.686	1.474	0.000006	0.000006	0.000001	0.98342
4	14.024	9.258	1.589	0.000050	0.000048	0.000006	0.98381

Table 3 Results of non-linear regression analysis for DDS

R_y	a_0	a_1	a_2	$\lvert\varepsilon_0\rvert$	$\lvert\varepsilon_1\rvert$	$\lvert\varepsilon_2\rvert$	R^2
1.5	8.403	20.466	1.534	0.000037	0.000018	0.000000	0.98771
2	21.051	15.812	2.204	0.000023	0.000014	0.000001	0.98916
2.5	29.273	12.708	3.066	0.000041	0.000030	0.000002	0.98335
3	38.657	10.999	4.060	0.000020	0.000017	0.000002	0.98336
3.5	46.591	9.686	5.158	0.000086	0.000080	0.000010	0.98342
4	56.097	9.258	6.354	0.000041	0.000039	0.000005	0.98381

The input for iteration step $(k+1)$ (i.e., the next iteration step) is obtained as in Eq. (11):

$$\{a\}_{k+1} = \{a\}_k + \{\Delta A\} \tag{11}$$

where $\{a\}$ is a 3-dimensional vector of a_0, a_1, and a_2 (i.e., constant parameters).

The iteration of GNA is performed until meets the convergence criteria for the absolute error related to constant parameters of Eq. (5). In this study, the convergence criterion is taken to be $|\varepsilon|_k = 10^{-4}$ for the iterative solution of nonlinear regression analysis.

Microsoft Excel-based spreadsheet tool for facilitating the iterative processes of GNA is developed by the Authors. The resulting constant parameters of Eq. (5), the absolute errors of the constant parameters computed at the last two steps of the iteration (ε_0, ε_1, and ε_2), and the correlation coefficients (R^2) between the computed and the estimated data are summarised in Tables 2 and 3 for the mean IDRS and the mean DDS, respectively. Six digits after the decimal point are shown in absolute errors of constant parameters to clearly demonstrate that absolute errors are smaller than 10^{-4}.

It is apparent from Tables 2 and 3 that all correlation coefficients are greater than 98%. Accordingly, a strong correlation between the computed and the estimated data is observed. In addition, the iterative data in Tables 2 and 3 indicates that sufficient convergence criteria for constant parameters of Eq. (5). are provided. Finally, the estimated inelastic displacement ratio and ductility demand spectra (DDS) are plotted in red in Figs. 9 and 10, respectively, together with the computed ones (i.e., the spectra plotted in black in Fig. 9 and the spectra plotted in blue in Fig. 10). It is obvious that there is a good agreement between the computed and estimated spectra. The results of the final part of this study encourage further efforts to develop DDS for design purposes in consideration of pulse-like GMs.

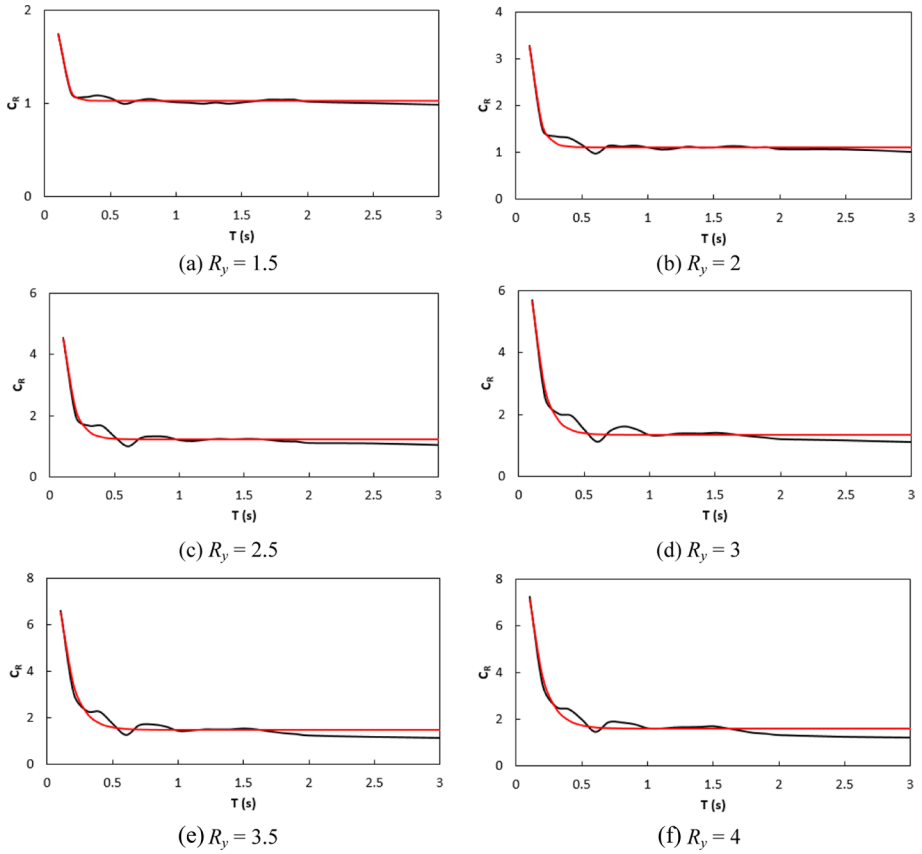

Fig. 9 Computed and estimated mean IDRS

5 Conclusions

Inelastic displacement ratio and displacement ductility demand spectra (DDS) for stiffness-degrading SDOF systems subjected to pulse-like GMs of the 2023 Pazarcık (Kahramanmaraş) earthquake are computed by nonlinear RHA. The ductility demands that cause structural damage and collapse in the regions affected by this devastating event are revealed. Computed inelastic displacement ratio and displacement ductility demand spectra (DDS) are subsequently estimated by the GNA. The following conclusions can be drawn:

(1) Pulse-like GMs recorded during the 2023 Pazarcık (Kahramanmaraş) earthquake have imposed large IDRs.
(2) Relatively high ductility demands are imposed on highly inelastic systems.
(3) Local amplification of mean inelastic displacement ratio and ductility demand spectra (DDS) are observed at periods of vibration around 0.7–0.8 s.
(4) The well-known EDR may result in significant underestimations of the maximum inelastic displacement demands of the considered pulse-like GMs since the mean inelastic displacement ratios are larger than 1.0 at intermediate and long periods.

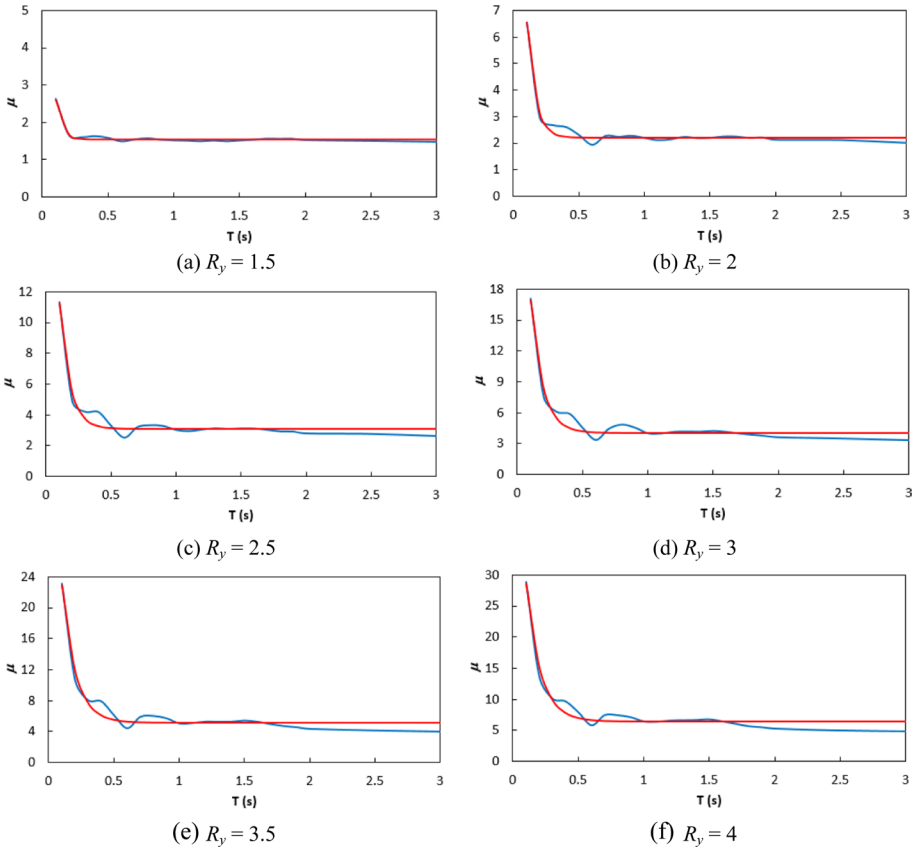

Fig. 10 Computed and estimated mean DDS

(5) At relatively long periods, ductility demands do not exactly approximate to lateral strength ratios, which means that DDS do not exhibit the typical spectral shape.
(6) For seismic design and evaluation purposes, the modification of elastic displacements alone may not be enough to adequately estimate inelastic displacements.
(7) Simple but quite efficient predictive models for both inelastic displacement ratio and displacement ductility demand spectra (DDS) are developed. The predictive model provides a strong correlation between the computed and the estimated data.
(8) Both inelastic displacement ratio and ductility demand spectra (DDS) do not exhibit the trend of spectra of SDOF systems subjected to ordinary GMs.

The results of this study overall indicate the necessity of involving pulse-like GMs in next-generation earthquake codes. The effectiveness of the predictive models developed herein might encourage further efforts to develop DDS for design purposes.

Author contributions TU: Conceptualization, Data collection and analysis, Writing original draft. Corrections for the revised manuscript. OM: Writing and editing, Commenting on the manuscript. Corrections for the revised manuscript.

Funding Open access funding provided by the Scientific and Technological Research Council of Türkiye (TÜBİTAK). The authors declare that no funds, grants, or other support were received during the preparation of this manuscript.

Data availability All data and models analysed during the current study are available from the corresponding author on reasonable request.

Declarations

Conflict of interest The authors have no relevant financial or non-financial interests to disclose.

References

AFAD (2023) Disaster and emergency management presidency (Available from: https://tadas.afad.gov.tr/list-waveform)

Akkar SD, Miranda E (2005) Statistical evaluation of approximate methods for estimating maximum deformation demands on existing structures. J Struct Eng 131(1):160–172. https://doi.org/10.1061/(ASCE)0733-9445(2005)131:1(160)

Alavi B, Krawinkler H (2004) Behavior of moment-resisting frame structures subjected to near-fault ground motions. Earthq Eng Struct Dyn 33(1):687–706. https://doi.org/10.1002/eqe.369

Aschheim M, Black E (1999) Effects of prior earthquake damage on response of simple stiffness-degrading structures. Earthq Spectra 15(1):1–24. https://doi.org/10.1193/1.1586026

Aydemir ME (2013a) Soil structure interaction effects on structural parameters for stiffness degrading systems built on soft soil sites. Struct Eng Mech 45(5):655–676. https://doi.org/10.12989/sem.2013.45.5.655

Aydemir ME (2013b) Inelastic displacement ratios for evaluation of stiffness degrading structures with soil structure interaction built on soft soil sites. Struct Eng Mech 45(6):741–758. https://doi.org/10.12989/sem.2013.45.6.741

Baéz JI, Miranda E (2000) Amplification factors to estimate inelastic displacement demands for the design of structures in the near field. In: Proceedings of the 12th world conference on earthquake engineering, Auckland, New Zealand

Baker JW (2007) Quantitative classification of near-fault ground motions using wavelet analysis. Bull Seism Soc Am 97(5):1486–1501. https://doi.org/10.1785/0120060255

Baltzopoulos G, Vamvatsikos D, Iervolino I (2016) Analytical modelling of near-source pulse-like seismic demand for multi-linear backbone oscillators. Earthq Eng Struct Dyn 45(11):1797–1815. https://doi.org/10.1002/eqe.2729

Baltzopoulos G, Baraschino R, Chioccarelli E, Cito P, Vitale A, Iervolino I (2023) Near-source ground motion in the M7.8 Gaziantep (Turkey) earthquake. Earthq Eng Struct Dyn 52(12):3903–3912. https://doi.org/10.1002/eqe.3939

Boore DM, Watson-Lamprey J, Abrahamson NA (2006) Orientation-independent measures of ground motion. Bull Seismol Soc Am 96(4A):1502–1511. https://doi.org/10.1785/0120050209

Chopra AK, Kan C (1973) Effects of stiffness degradation on ductility requirements for multistorey buildings. Earthq Eng Struct Dyn 2(1):35–45. https://doi.org/10.1002/eqe.4290020104

Dong H, Han Q, Bi K, Zhang C, Du X (2022) Ductility demand spectra of the self-centering structure subjected to near-fault pulse-like ground motions. J Earthq Eng 26(12):6129–6147. https://doi.org/10.1080/13632469.2021.1911886

Farrow KT, Kurama YC (2004) SDOF displacement ductility demands based on smooth ground motion response spectra. Eng Struct 26(12):1713–1733. https://doi.org/10.1016/j.engstruct.2004.06.003

FEMA P440A (2009) Effects of strength and stiffness degradation on seismic response. Federal Emergency Management Agency, Washington

Ganjavi B, Bararnia M, Hajirasouliha I (2018) Seismic response modification factors for stiffness degrading soil-structure systems. Struct Eng Mech 68(2):159–170. https://doi.org/10.12989/sem.2018.68.2.159

Hassani N, Bararnia M, Amiri GG (2018) Effect of soil-structure interaction on inelastic displacement ratios of degrading structures. Soil Dyn Earthq Eng 104:75–87. https://doi.org/10.1016/j.soildyn.2017.10.004

Hatzigeorgiou GD (2010) Ductility demand spectra for multiple near- and far-fault earthquakes. Soil Dyn Earthq Eng 30(4):170–183. https://doi.org/10.1016/j.soildyn.2009.10.003

Iervolino I, Chioccarelli E, Baltzopoulos G (2012) Inelastic displacement ratio of near-source pulse-like ground motion. Earthq Eng Struct Dyn 41(15):2351–2357. https://doi.org/10.1002/eqe.2167

Işık E, Avcil F, Arkan E, Büyüksaraç A, İzol R, Topalan M (2023) Structural damage evaluation of mosques and minarets in Adıyaman due to the 06 February 2023 Kahramanmaraş earthquakes. Eng Fail Anal 151:107345. https://doi.org/10.1016/j.engfailanal.2023.107345

Ji K, Ren Y, Wen R, Kuo C-H (2019) Near-field velocity pulse-like ground motions on February 6, 2018 M_W6.4 Hualien, Taiwan earthquake and structural damage implications. Soil Dyn Earthq Eng 162:105784. https://doi.org/10.1016/j.soildyn.2019.105784

Kalkan E, Kunnath SK (2006) Effects of fling step and forward directivity on seismic response of buildings. Earthq Spectra 22(2):367–390. https://doi.org/10.1193/1.2192560

Kalkan E, Reyes JC (2015) Significance of rotating ground motions on behavior of symmetric-and asymmetric-plan structures: Part II. Multi-story structures. Earth Spec 31:1613–1628. https://doi.org/10.1193/072012Eqs242M

Li C, Kunnath S, Zou Z, Peng W, Zhai C (2020a) Effects of early-arriving pulse-like ground motions on seismic demands in RC frame structures. Soil Dyn Earthq Eng 130:105997. https://doi.org/10.1016/j.soildyn.2019.105997

Li C, Zuo Z, Kunnath S, Chen L (2020b) Orientation of the strongest velocity pulses and the maximum structural response to pulse-like ground motions. Soil Dyn Earthq Eng 136:106240. https://doi.org/10.1016/j.soildyn.2020.106240

Li C, Kunnath S, Zhai C (2020c) Influence of early-arriving pulse-like ground motions on ductility demands of single-degree-of-freedom systems. J Earthq Eng 24(9):1337–1360. https://doi.org/10.1080/13632469.2018.1466744

Lu Y, Hajirasouliha I, Marshall AM (2018) Direct displacement-based seismic design of flexible-base structures subjected to pulse-like ground motions. Eng Struct 168:276–289. https://doi.org/10.1016/j.engstruct.2018.04.079

Ozkula G, Dowell RK, Baser T, Lin J-L, Numanoglu OA, Ilhan O, Olgun CG, Huang C-W, Uludag TD (2023) Field reconnaissance and observations from the February 6, 2023, Turkey earthquake sequence. Nat Hazard 119:663–700. https://doi.org/10.1007/s11069-023-06143-2

Ozturk M, Arslan MH, Korkmaz HH (2023) Effect on RC buildings of 6 February 2023 Turkey earthquake doublets and new doctrines for seismic design. Eng Fail Anal 153:107521. https://doi.org/10.1016/j.engfailanal.2023.107521

Pekoz HA, Pincheira JA (2004) Seismic response of strength and stiffness degrading single degree of freedom systems. In: Proceedings of 13th world conference on earthquake engineering, Vancouver, BC

Pincheira JA, Song J-K (2000) Displacement amplification factors for degrading systems subjected to near-fault ground motions. In: Proceedings of 12th world conference on earthquake engineering, Auckland, New Zealand

PRISM (2010) A software for seismic response analysis of single-degree-of-freedom-systems. INHA University, Earthquake Engineering Department of Architectural Engineering

Reyes JC, Kalkan E (2012) Relevance of fault-normal/parallel and maximum direction rotated ground motions on nonlinear behavior of multi-story buildings. 15th World Conference on Earthquake Engineering, Lisboa, Portugal

Ruiz-García J (2011) Inelastic displacement ratios for seismic assessment of structures subjected to forward-directivity near-fault ground motions. J Earthq Eng 15(3):449–468. https://doi.org/10.1080/13632469.2010.498560

Ruiz-Garcia J, Miranda E (2003) Inelastic displacement ratios for evaluation of existing structures. Earthq Eng Struct Dyn 32(8):1237–1258. https://doi.org/10.1002/eqe.271

Sagbas G, Garjan RS, Sarikaya K, Deniz D (2023) Field reconnaissance on seismic performance and functionality of Turkish industrial facilities affected by the 2023 Kahramanmaras earthquake sequence. Bull Earthq Eng. https://doi.org/10.1007/s10518-023-01741-8

Sehhati R, Rodriguez-Marek A, ElGawady M, Cofer WF (2011) Effects of near-fault ground motions and equivalent pulses on multi-story structures. Eng Struct 33(3):767–779. https://doi.org/10.1016/j.engstruct.2010.11.032

Song J-K, Pincheira JA (2000) Spectral displacement demands of stiffness- and strength-degrading systems. Earthq Spectra 16(4):817–851. https://doi.org/10.1193/1.1586141

Takeda T, Sozen MA, Nielsen NN (1970) Reinforced concrete response to simulated earthquakes. J Struct Div 96(12):2557–2573. https://doi.org/10.1061/JSDEAG.0002765

Tao W, Jie C, Yujiang Z, Xiaoqing W, Xuchuan L, Xiaoting W, Qingxue S (2023) Preliminary investigation of building damage in Hatay under February 6, 2023 Turkey earthquakes. Earthq Eng Eng Vib. https://doi.org/10.1007/s11803-023-2201-0

TBEC (2018) Türkiye Building Earthquake Code (in Turkish). Ministry of Interior Disaster and Emergency Management Presidency, Ankara, Türkiye

Uçar T, Merter O (2020) Inelastic strength and ductility demand of M_w 6.9 Samos Island (Aegean Sea) earthquake. In: Proceedings of 6th international conference on earthquake engineering and seismology, Gebze, Kocaeli, Turkey

Ucar T, Merter O (2022) Predictive model for constant-ductility energy factor spectra of near- and far-fault ground motions based on Gauss-Newton algorithm. J Earthq Eng 26(15):7689–7714. https://doi.org/10.1080/13632469.2021.1964653

Vuran E, Serhatoğlu C, Timurağaoğlu MÖ, Smyrou E, Bal İE, Livaoğlu R (2024) Damage observations of RC buildings from 2023 Kahramanmaraş earthquake sequence and discussion on the seismic code regulations. Bull Earthq Eng. https://doi.org/10.1007/s10518-023-01843-3

Wen W-P, Zhai C-H, Li S, Chang Z, Xie L-L (2014) Constant damage inelastic displacement ratios for the near-fault pulse-like ground motions. Eng Struct 59:599–607. https://doi.org/10.1016/j.engstruct.2013.11.011

Wu F, Xie JJ, An Z, Lyu CH, Taymaz T, Irmak TS, Li XJ, Wen ZP, Zhou BF (2023) Pulse-like ground motion observed during the 6 February 2023 $MW_{7.8}$ Pazarcık Earthquake (Kahramanmaraş, SE Türkiye). Earthq Sci 36(4):328–339. https://doi.org/10.1016/j.eqs.2023.05.005

Yang T, Yuan X, Zhong L, Yuan W (2023) Near-fault pulse seismic ductility spectra for bridge columns based on machine learning. Soil Dyn Earthq Eng 164:107582. https://doi.org/10.1016/j.soildyn.2022.107582

Yi W-J, Zhang H-Y, Kunnath SK (2007) Probabilistic constant-strength ductility demand spectra. J Struct Eng 133(4):567–575. https://doi.org/10.1061/(ASCE)0733-9445(2007)133:4(567)